Proceedings of the Twenty-eighth (2018) International Ocean and Polar Engineering Conference **www.isope.org**
Sapporo, Japan, June 10-15, 2018

ISBN 978-1-880653-87-6; ISSN 1098-6189

Comparative Study of SST-SAS and SST-DDES in Predicting Massively Separated Flow

*Di Wu, Weiwen Zhao, Decheng Wan**
Collaborative Innovation Center for Advanced Ship and Deep-Sea Exploration, State Key Laboratory of Ocean Engineering, School of Naval Architecture, Ocean and Civil Engineering, Shanghai Jiao Tong University, Shanghai, China
*Corresponding author

ABSTRACT

The main objective of this paper is to evaluate the capability of SST-SAS and SST-DDES to predict massively separated flow. Flow past a circular cylinder at subcritical Reynolds number Re = 3900 is numerically studied. The hybrid characters of SAS and DDES are discussed in principle. Some typical results such as velocity profiles are calculated. Additionally, the effect of the L_{vk} limiter on the performance of SST-SAS is discussed. Both SST-SAS and SST-DDES achieve results in favorable agreement with the experiment data. However, a finer mesh generation is needed for SST-SAS, which means that SST-SAS still remains improvements.

KEY WORDS: Scale-Adaptive Simulation; Delayed-Detached Eddy Simulation; circular cylinder; subcritical Reynolds number; flow separation;

INTRODUCTION

Flow around a circular cylinder is usually treated as one of the most classic cases in which the massively separated flow appears behind bluff bodies. It has complex features such as laminar boundary-layer separation and periodic vortex shedding despite of the simplicity of geometry. Hence, it is challenging to accurately predict such an unsteady flow phenomenon with economical computation cost. Reynolds-Averaged Navier-Stokes (RANS) equation is always in favor of its cheap cost. However, it is also blamed for its bad performance in predicting massively separated flow due to its incapability of resolving instantaneous small turbulence scales. While direct numerical simulation (DNS) and wall-resolved large-eddy simulation (LES) are supposed to possess high simulation accuracy, their computation cost is too expensive to be afforded. Hybrid RANS/LES method combines the advantages of RANS and LES by simulating the near wall flow region with RANS and the separated flow region with LES. Hence, hybrid RANS/LES method is widely used to predict massively separated flows in current engineering applications.

Detached-eddy simulation (DES) is one of the mostly used hybrid RANS/LES method due to its simplicity in formulation and adaptation in complex geometry. Recently, several investigations have been carried out to validate the capability of DES to be industrial (Zhao, 2016). The first DES model DES97 proposed by Spalart (1997) substitutes the wall distance with the grid scale when the grid is adequately fine for LES simulation. However, DES97 model suffers several problems including the undefined "grey area" inside the RANS/LES interface. One of the most serious problem faced by DES is the modeled stress depletion (MSD) problem. It occurs when the grid is fine enough for activating LES branch but not fine enough to resolve the turbulence fluctuations internal to boundary layers. As a result, MSD leads to the unphysically grid-induced separation. To address this drawback, delayed-detached eddy simulation (DDES) modifies the character length scale to protect the RANS region from being prematurely switched into LES region. However, this kind of modification is incapable of completely preventing the occurrence of MSD problem, which is just postponed to a finer grid spacing as commented by Menter and Egorov (2005).

Another popular hybrid RANS/LES method is scale-adaptive simulation (SAS) proposed by Menter (2003). It introduces the von Karman length scale, which can dynamically adjust itself to the unsteadiness in the flowfield, into the turbulence model. Thus SAS achieves the hybrid characteristic without explicit grid dependence. In the region where the unsteadiness is relatively strong, SAS adaptively reduces eddy-viscosity so that small turbulence structures are resolved and a LES-like performance is obtained. What should be mentioned is that SAS has a pure RANS nature because it is originated from the two equation turbulence model derived by Rotta (1968). This characteristic of SAS leads to the need of rethinking about the definition of RANS. Meanwhile, SAS is considered as the representation of the so-called "the 2nd-generation URANS". However, the capability of SAS to predict massively separated flow should be investigated before being industrial (Stamou and Papadonikolaki, 2009). To systematically validate the performance of SAS, the widely used hybrid RANS/LES model DDES is presented in this paper for comparison. In the current work, the performance of SAS and DDES on simulating flow around a circular cylinder at subcritical Reynold number Re = 3900 is comparatively

studied. Here the two-equation SST model are operated in RANS mode both in SAS and DDES models.

NUMERICAL METHODS

Delayed detached eddy simulation

The main idea of DES is redefining the turbulence length scale which is contained in the dissipative term of the turbulence kinetic energy transport equation. The turbulence length scale defined in the SST-DES (Strelets, 2001) model is as follows:

$$L_{DES} = \min(L_{RANS}, L_{LES}) \tag{1}$$

where $L_{RANS} = \sqrt{k}/(C_\mu \omega)$ is the RANS turbulence length scale, and $L_{LES} = C_{DES}\Delta$ is the LES length scale, i.e. local grid scale.

In the near wall region, the RANS turbulence length scale is supposed to be smaller than local grid scale, so that its original definition is maintained and RANS branch is activated. While the turbulence motions develop far from wall where local grid is fine enough to support LES branch, the RANS turbulence length scale is substituted by local grid scale and LES branch is activated. As a result, the dissipative term is increased following by eddy-viscosity being decreased, and smaller turbulence structures are resolved. The hybrid characteristic of DES is relied on comparing the RANS character length scale and local grid scale. Hence, the switch of RANS region to LES region is quite smooth, but inadequate to be safe. As mentioned in the introduction, when the LES branch is activated in the RANS region where local grid is too coarse to support LES, eddy-viscosity is incorrectly deceased and unphysical flow separation prematurely occurs, which is known as MSD problem

To protect RANS region from being invaded by LES region, DDES modified the character turbulence length scale by introducing the delay function. The delay function proposed by Spalart (2006) takes the form:

$$f_d = 1 - \tanh((8r_d)^3) \tag{2}$$

where $r_d = \frac{\nu_t + \nu}{\sqrt{u_{ij}u_{ij}}\kappa^2 d^2}$ is the delay factor. In the near wall boundary layer, f_d is equal to 0. While in the separated region far from wall, f_d approaches 1. The RANS turbulence length scale of DDES version is defined as

$$L_{DDES} = L_{RANS} - f_d \max(0, L_{RANS} - L_{LES}) \tag{3}$$

One can see that L_{DDES} is promised to be L_{RANS} in the boundary layer where is supposed to be covered by RANS region.

Based on Menter (1994) SST two-equation model, one can obtain SST-DDES model as

$$\frac{\partial}{\partial t}(\rho k) + \frac{\partial}{\partial x_i}(\rho u_i k) = P_k - C_\mu \rho k \omega F_{DDES} + \frac{\partial}{\partial x_i}[(\mu + \sigma_k \mu_t)\frac{\partial k}{\partial x_i}] \tag{4}$$

$$\frac{\partial}{\partial \mathrm{t}}(\rho \omega) + \frac{\partial}{\partial x_i}(\rho u_i \omega) = \frac{\rho \alpha}{\mu_t} P_k - C_\mu \rho \omega^2 + \frac{\partial}{\partial x_i}\left[(\mu + \sigma_\omega \mu_t)\frac{\partial \omega}{\partial x_i}\right] + 2(1 - F_1)\rho \sigma_{\omega 2} \frac{1}{\omega} \cdot \frac{\partial k}{\partial x_i} \cdot \frac{\partial \omega}{\partial x_i} \tag{5}$$

where F_{DDES} is defined as

$$F_{\mathrm{DDES}} = \max[\frac{L_{RANS}}{L_{LES}} f_d, 1] \tag{6}$$

Scale adaptive simulation

Different from SST-DDES which remedies the dissipative term in the turbulence kinetic energy transport equation, SST-SAS (Egorov and Menter, 2008) adds a scale-adaptive source term Q_{SAS} into the turbulence dissipation rate transport equation to achieve its hybrid character. The term Q_{SAS} is constructed as

$$Q_{SAS} = \max[\rho \zeta_2 \kappa S^2 \left(\frac{L}{L_{vk}}\right)^2 - C \cdot \frac{2\rho k}{\sigma_\phi} \max\left(\frac{|\nabla \omega|^2}{\omega^2}, \frac{|\nabla k|^2}{k^2}\right), 0] \tag{7}$$

where $L = \sqrt{k}/(c_\mu^{1/4} \cdot \omega)$ is the turbulence length scale and $L_{vk} = \frac{\kappa S}{|\nabla^2 U|}$ is the von Karman length scale.

The original meaning of L_{vk} is the characteristic length scale which represents the thickness of a two-dimensional boundary layer (Zheng, et al, 2016). The one contained in SST-SAS is the three-dimensional version of L_{vk} which can be read as the first derivative of velocity divided by the second derivative of velocity. As can be deduced from its definition, L_{vk} is sensitive to the unsteadiness in the flowfield. When the flowfield is quite steady such as what happens in the region inside boundary layer, L_{vk} is quite large and the source term Q_{SAS} is equal to 0. As soon as the unsteadiness develops in the flowfiled, L_{vk} adaptively decreases and Q_{SAS} activates in the turbulence dissipation rate transport equation to rise turbulence dissipation. Then the eddy viscosity correspondingly declines and more small turbulence scales are resolved, which can be seen as a LES-like behavior.

Because L_{vk} dynamically adjusts itself to the resolved turbulence scales, the hybrid characteristic of SAS is relied on the flow field and no explicit grid dependence is needed. What should be mentioned is that SAS is unable to resolve turbulence scales down to the local grid limit. However, sometimes L_{vk} is smaller than the grid scale, causing the turbulence energy contained in the high wave number turbulence motions to accumulate. Hence, a limiter is needed to confine L_{vk} for correctly dissipating the energy contained in the finest resolved turbulence fluctuations. The L_{vk} limiter constructed by restrict the equilibrium eddy viscosity of SST-SAS with the eddy viscosity of LES Smagorinsky model (Smagorinsky, 1963) can be obtained as

$$L_{vk} = \max(\frac{\kappa S}{|\nabla^2 U|}, C_s \sqrt{\kappa \zeta_2 / ((\beta / C_\mu) - \alpha)} \cdot \Delta) \tag{8}$$

All the coefficients and the details contained in SST-DDES model and SST-SAS model can be found in the papers (Menter, et al, 2003) and (Menter and Egorov, 2010).

NUMERICAL DETAILS

Numerical schemes

All the computations presented in this paper is carried out on the open source platform OpenFOAM. The Naiver-Stokes equations are discretized by using a cell-centered finite-volume method based on block-structured grids. The implicit Euler scheme is adopted to discretize the unsteady time integration. The convective term is discretized by linear TVD scheme with a limiter, while the diffusive term is discretized by Gauss linear conservation scheme. The coupled velocity and pressure is dealt by applying the PIMPLE algorithm.

Computational domain

As can be seen in Fig. 1, the diameter of the circular cylinder is set to be D = 0.01m, and the height is set to be $L_Z = \pi D$ as described by

Kravchenko (2000). The origin of coordinates is set at the center of the circular cylinder. The length of the computational domain in the flow direction is arranged as 45*D*, while 30*D* is set for the vertical direction. This form of domain arrangement is to ensure the full characteristics of flow past a circular cylinder can be completely captured.

Boundary conditions

According to the physics feature, the boundary is marked as the inlet, the outlet, the sides, the bottom and the top. The surface of the cylinder is considered as a no-slip wall. At the inlet boundary, a uniform incoming flow with velocity equal to the free stream velocity $U_\infty = 0.039m \cdot s^{-1}$ is defined. At the outlet boundary, the pressure gradient is set equal to 0. The rest of the boundaries is defined as symmetry boundary, assuming that the height of the cylinder is infinite.

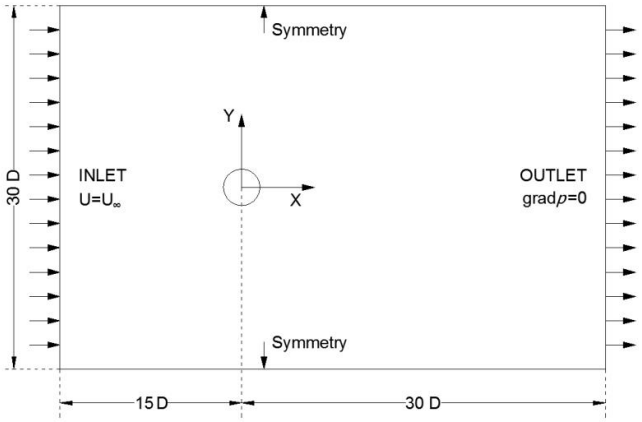

Fig. 1 Computational domain and boundary conditions

Mesh generation

Structured mesh generation is chosen in this case because of the simple geometry of the cylinder. As shown in Fig. 2, the mesh domain of 5*D* around the cylinder is generated with the O block grids. While the rest of mesh domain is generated with orthogonal hexahedral grids. The thickness of the first grid near the wall of the cylinder is set as $\Delta = 0.005D$ to ensure that $y^+ \leq 1$. The grid nodes distributed in the span-wise direction is set to be $n_Z = 32$ for a coarse mesh, $n_Z = 48$ for a medium mesh and $n_Z = 64$ for a fine mesh, with the total number of grid units being 850K, 1.4M and 2.3M, respectively. As can be seen in Table 1, the results of SST-DDES in these three meshes vary slightly, so the result of SST-DDES in the coarse mesh can be thought as mesh independent. While the results of SST-SAS in the coarse mesh differ far away from which obtained in the other two meshes, so the result of SST-SAS in the medium mesh is adopted for adequate accuracy. This discrepancy could be due to that SST-DDES divides RANS region and LES region explicitly, while the division criteria of SST-SAS is dependent on the flowfield.

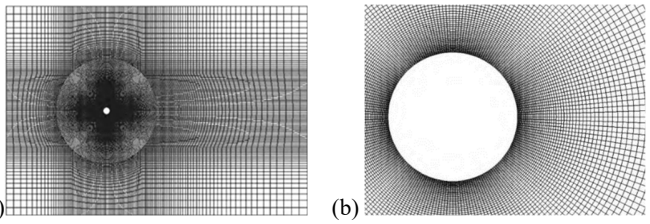
(a) (b)
Fig. 2 Global and local mesh for a circular cylinder. (a) Global mesh. (b) Local mesh

Table 1. Overall flow parameters of the flow past a circular cylinder

Data Source	N_{total}	C_d	$-C_{pb}$	S_t	L_{rec}/D	U_{min}/U_∞
Experiment	-	0.99	0.88	0.215	1.33	0.24
PIV	-	-	-	0.208	1.51	0.34
LES	2.4M	-	-	0.208	1.56	0.26
SST-DDES	850K	1.00	0.84	0.208	1.52	0.29
SST-DDES	1.4M	0.99	0.86	0.209	1.50	0.28
SST-DDES	2.3M	0.99	0.85	0.208	1.51	0.26
SST-SAS	850K	1.21	0.96	0.221	1.05	0.20
SST-SAS	1.4M	1.03	0.85	0.207	1.75	0.28
SST-SAS	2.3M	1.02	0/87	0.208	1.73	0.26

RESULTS AND DISCUSSIONS

To compare the performance of SST-DDES model and SST-SAS model, some classic experiment data is presented in this paper. The pressure coefficients along the surface of the cylinder measured by Norberg (1994) and the PIV experiments of the velocity in the near wake of the cylinder ($x/D < 3.0$) and the velocity outside the recirculation region ($3 < x/D < 10$) carried out by Parnaudeau (2008) are included. In addition, the predictions of the very good LES simulated by Krachenko and Moin (2000) is also presented in this paper for a detailed comparison.

Time-averaged results

Some typical values of the overall flow parameters such as the drag coefficient C_d and the period of shedding S_t are presented together with experimental values and LES predictions in Table 1. The total averaged time is about 78 periods of vortex shedding, which is considered to be long enough for the average operations.

Compared with the experiments data, one can see that the overall flow parameters predicted by both SST-DDES and SST-SAS are admirably accuracy. The performance of both these two models is considered to be quite close to the performance of LES. However, it should be noticed that the recirculation region predicted by SST-SAS is a little longer than SST-DDES and LES.

The distributions of normalized pressure coefficient around the surface of the cylinder compared with the experiment value (Norberg, 1994) is shown in Fig. 3. It can be seen that the pressure reaches its maximum value at the upstream stagnation point, then is reduced down to its minimum before recovers to a constant value which is known as the base pressure C_{pb}. The pressure coefficients on the surface of the cylinder predicted by both SST-SAS and SST-DDES excellently match the experiment values, while the prediction of SST-SAS can be seen as superior than SST-DDES from $\theta = 60°$ to $\theta = 175°$.

The cross-stream profiles of the mean velocity components are plotted for the analysis of the time-averaged flowfield. The normalized mean stream-wise velocity U/U_∞ in the near wake of the cylinder ($x/D < 3.5$) is plotted in Fig. 4. Quite close to the PIV data, both SST-SAS and SST-DDES can predict a symmetrical U-shape profile of U/U_∞ in the wake near the cylinder (x/D = 1.06) and a V-shape profile of U/U_∞ downstream. And the prediction of SST-DDES matches the PIV data excellently except some tiny discrepancies around the inflection points. However, the minimum value of U/U_∞ in x/D = 1.06 predicted by SST-SAS is lower than SST-DDES, leading to a more "plump" shape of the U/U_∞ profile and greater discrepancies compared with the PIV data. This indicates that the recirculation region calculated by SST-SAS

should be larger than SST-DDES and the PIV data, as shown in Table. 1. In general, the near wake stream-wise velocity predictions of both SST-SAS and SST-DDES are satisfactory.

As can be seen in Fig. 5, the normalized mean cross-flow velocity V/U_∞ in the near wake predicted by SST-DDES fits the PIV data quite well expect a lower maximum value. While compared with SST-DDES, SST-SAS overpredicts the cross-flow velocity in x/D = 1.06 and then underpredicts the cross-flow velocity in x/D = 1.54 and x/D = 2.02, leading to the relatively large mismatches with the PIV data. It can be speculated that there exists more turbulence mixing predicted by SST-SAS in the near wake region compared with SST-DDES.

The normalized mean stream-wise velocity U/U_∞ in the far wake of the cylinder ($x/D \leq 10$) is plotted in Fig. 6. Obviously, SST-DDES underpredicts the minimum value along the centerline of the cylinder compared with both SST-SAS and the PIV data. It could be due to the rather large grid spacing in the far wake of the cylinder. Contrastly, SST-SAS performs better than SST-DDES in the far wake with an admirably match with the experiment data. It means that compared with SST-SAS, SST-DDES overpredicts the dissipation of turbulence motions which develop from the near wake down to the far wake of the circular cylinder, meaning that the prediction of SST-SAS in the far wake is closer to the physical truth.

The cross-stream distributions of the mean normalized stream-wise Reynolds stresses in the near wake is also plotted in Fig. 7. The symmetrical profile is correctly predicted by both SST-SAS and SST-DDES. Compared with the PIV data, SST-DDES underpredicts the peak values, while it matches the experiment values better in the region near y/D = 1.0. On the contrary, the peak values predicted by SST-SAS are closer to the PIV data, while SST-SAS performs inferior to SST-DDES in predicting the flow region near y/D = 1.0. Associated with the performance of SST-SAS in predicting the profile of V/U_∞ in the near wake, it can be concluded that the turbulence motions predicted by SST-SAS in the near wake is actually more activated than SST-DDES.

Generally, the overall flow parameters predicted by both two hybrid RANS/LES model are admirable expect a little longer recirculation distance predicted by SST-SAS. While compared with the PIV data, the velocity profiles predicted by SST-DDES are more favorable than SST-SAS in the near wake region. And SST-SAS performs better in predicting the velocity profiles in the far wake region.

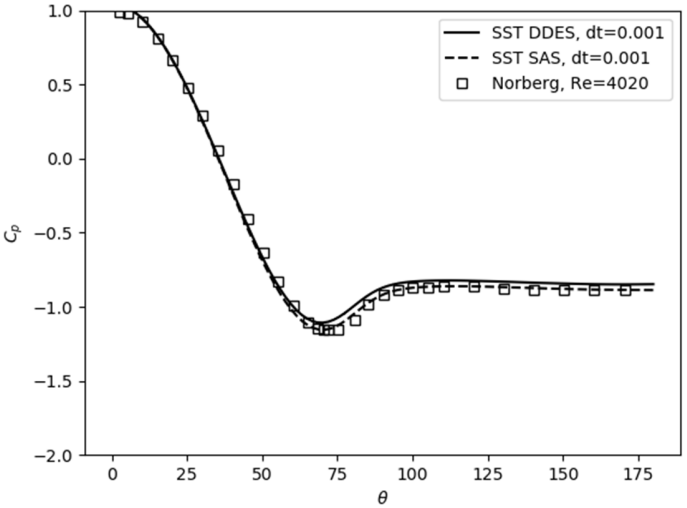

Fig. 3 Distributions of mean pressure coefficient on cylinder surface

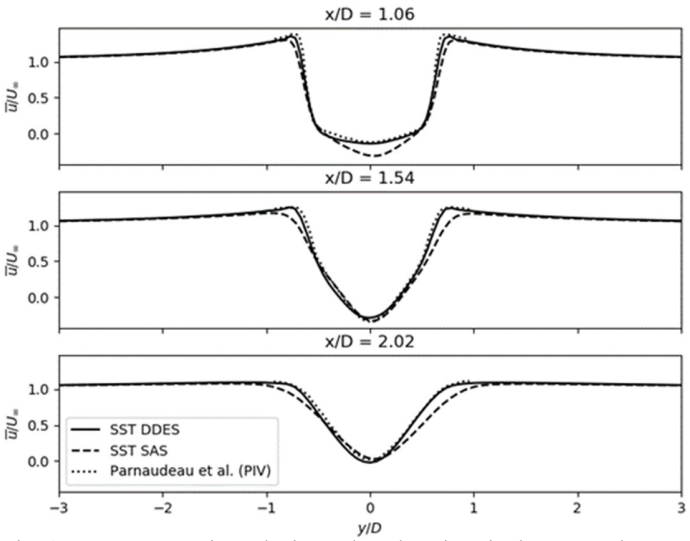

Fig. 4 Mean stream-wise velocity at three locations in the near wake

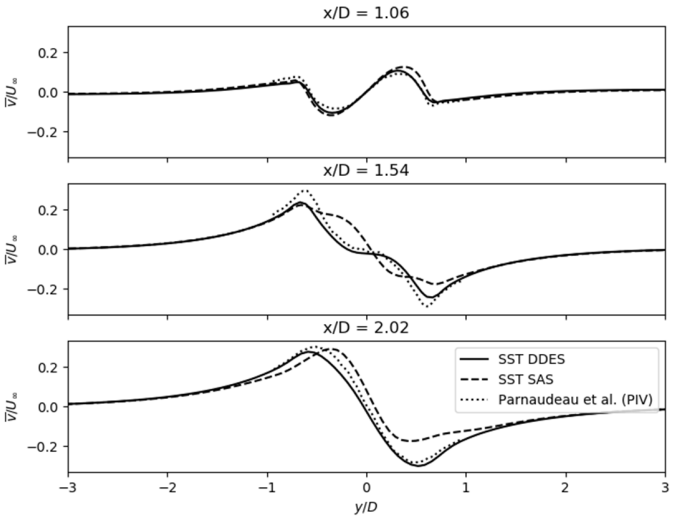

Fig. 5 Mean cross-flow velocity at three locations in the near wake

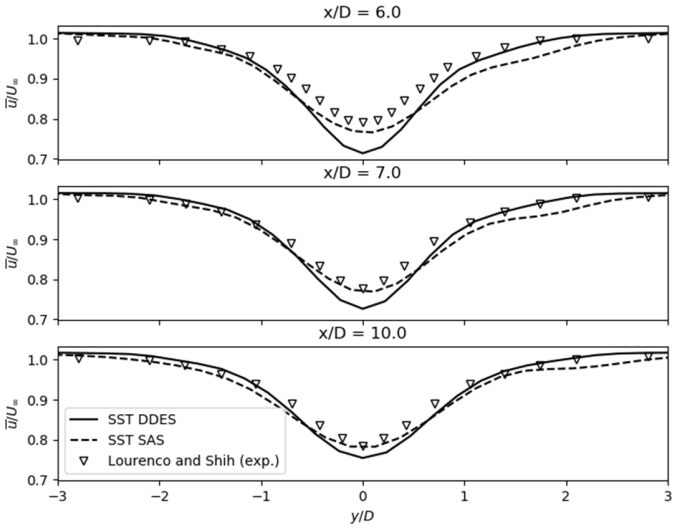

Fig. 6 Mean stream-wise velocity at three locations in the far wake

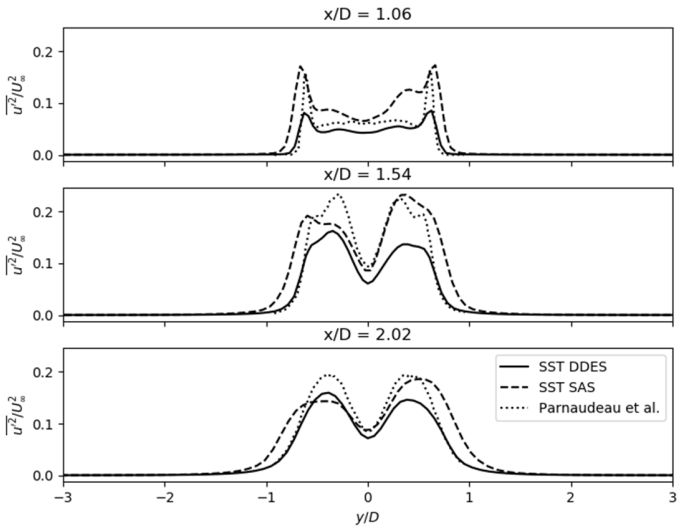

Fig. 7 Mean stream-wise normal Reynolds stresses in the near wake

Instantaneous flowfield

Fig. 8 depicts the instantaneous flow structures predicted by SST-SAS and SST-DDES. The visualization of the vortices is realized by displaying the iso-surface of the Q-criterion recommended by Hunt (1988), which is defined as follows:

$$Q = -\frac{1}{2}(S_{ij}S_{ij} - \Omega_{ij}\Omega_{ij}) \tag{9}$$

where S and Ω denote the strain of rate and rotation tensors, respectively. Both SST-SAS and SST-DDES can capture rather small turbulence structures and the irregular vortex shedding, showing their abilities to simulate 3D effect which RANS usually fails to simulate. Although both these two turbulence models exhibit similar hybrid RANS/LES characteristic, their hybrid mechanisms are quite different. As mentioned before, SAS has a pure URANS nature and the joint of the RANS region and the LES-like region is dependent on the characteristic of flowfiled. At the very beginning of simulation, SST-DDES quickly switches itself into the LES mode. In contrast, SST-SAS demonstrates near two dimensional turbulence structure, which can be described as "URANS-like" behavior, when the L_{vk} is so large that the Q_{SAS} term is nonactivated. Then along with the unsteadiness develops in the flowfield, L_{vk} decreases and Q_{SAS} increases so that smaller turbulence scales can be resolved and more evident 3D effect can be simulated as can be seen in Fig. 9.

Fig. 10 shows the iso-contour maps of the vorticity in the XY-plane. Compared with the results of LES in Fig. 11, one can notice that the transition region predicted by SST-SAS is larger than SST-DDES and similar to the results predicted by LES in fine grids. While the transition region predicted by SST-DDES is quite short which is similar to the results predicted by LES in coarse grids. Moreover, what can be seen is that the vorticity predicted by SST-SAS lasts longer distance downstream than SST-DDES, whose prediction of the vorticity dissipate rather fast downstream. This could explain that the unsatisfied performance of SST-DDES in predicting the far wake flowfield due to its excess dissipation there.

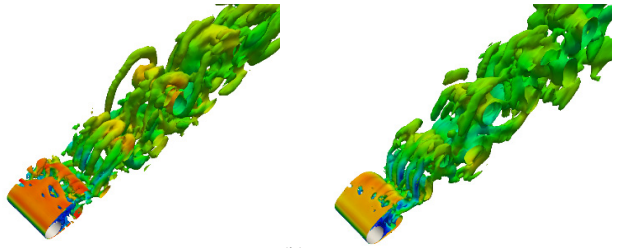
(a) (b)
Fig. 8 Iso-surface of the Q-criterion, flow past a circular cylinder. (a) SST-DDES simulation. (b) SST-SAS simulation

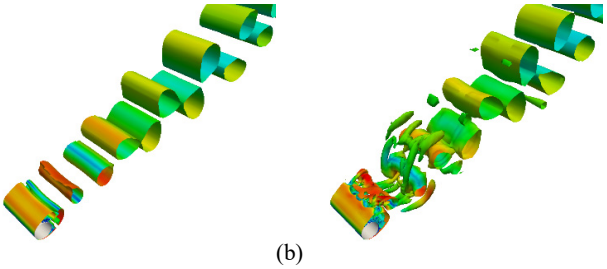
(a) (b)
Fig. 9 Iso-surface of the Q-criterion, flow past a circular cylinder, SAS simulation. (a) t = 1.2s. (b) t = 1.4s

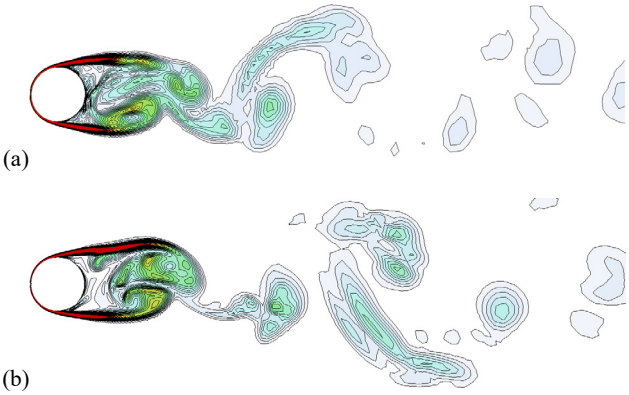
(a) (b)
Fig. 10 Contours of vorticity magnitudes of the flow past a cylinder in the X-Y plane. (a) SST-DDES simulation. (b) SST-SAS simulation

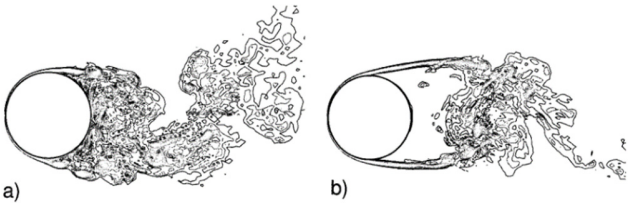
a) b)
Fig. 11 Contours of vorticity magnitudes of the flow past a cylinder in the X-Y plane (Kravchenko and Moin, 2000). Simulated with (a) LES in the coarse mesh and (b) LES in the fine mesh

The effect of the L_{vk} limiter on SST-SAS

As mentioned before, it is necessary to construct a limiter of the von Karman scale L_{vk} in case that L_{vk} is smaller than local grid scale when the unsteadiness in the flowfield is quite large. Otherwise, the finest scale turbulence fluctuations which is excess the resolution of local grid will fail to be correctly dissipated. Introduced by Menter and Egorov (2006), Smagorinsky model as the most classic LES model, is used to construct L_{vk} limiter with the eddy-viscosity constraint as described below:

$$\mu_t^{SAS} \geq \mu_t^{Smagorinsky} \tag{10}$$

where μ_t^{SAS} is the eddy-viscosity of SST-SAS model and the $\mu_t^{Smagorinsky}$ is the eddy-viscosity of Smagorisnky model. In fact, there exists considerable areas where L_{vk} is smaller than local grid scale. As a result, the eddy-viscosity of SST-SAS model is substituted with the eddy-viscosity of Smagorinsky model. Hence, the characteristics of Smagorinsky model is supposed to substantially influence the performance of SST-SAS. To preliminarily investigate the effect of the L_{vk} limiter on SST-SAS, here modifies the value of the Smagorsinky constant $C_s = 0.11$ contained in the L_{vk} limiter to be $C_s = 0.08$. The simulation of SST-SAS and its modified version is carried out in the coarse mesh. The coarse mesh is insufficient for SST-SAS to accurately predict the flow past a cylinder, but sufficient for SST-DDES as will be seen below.

It can be seen in Figs. 12~15 that the origin version of SST-SAS with $C_s = 0.11$ performed on the coarse mesh, under-predicts the distributions of normalized pressure coefficient around the surface of the cylinder. Moreover, the prediction of mean velocity distribution in the near wake and far wake is far less satisfactory compared with SST-DDES. In contrast, the prediction of the modified version of SST-SAS with $C_s = 0.08$ carried out in the same coarse mesh, is quite favorable as similar to the prediction of SST-DDES. These discrepancies indicate that the L_{vk} limiter indeed has a non-negligible effect on the performance of SST-SAS. Hence, this observation stimulates the need to elaborately investigate the effect of L_{vk} limiter on the performance of SST-SAS, especially the effect of the LES model used to construct the L_{vk} limiter.

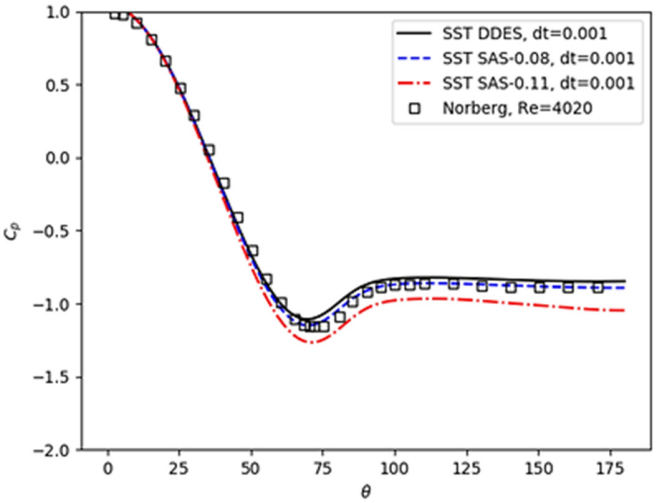

Fig. 12 Distributions of mean pressure coefficient on cylinder surface

CONCLUSION

To compare the capability of SST-SAS and SST-DDES to predict the massively separated flow, a 3D flow past a circular cylinder at subcritical Reynolds number Re = 3900 is numerically studied. In general, the prediction of both SST-SAS and SST-DDES is satisfactory compared with the experiment data. While SST-DDES performs better in the near wake region and SST-SAS shows its superiority in the far wake region. Moreover, both these two hybrid RANS/LES models are able to simulate small turbulence structures and 3D effect even though their hybrid mechanisms are quite different. However, compared with SST-DDES, SST-SAS needs a finer grid generation for accurate prediction, meaning that SST-SAS still remains improvements. Interestingly, when the

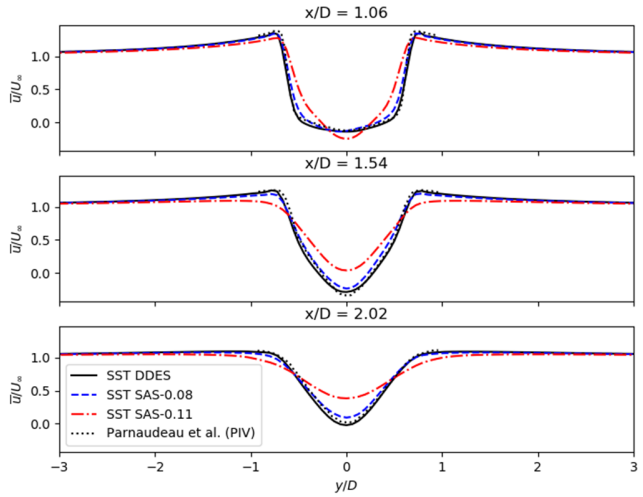

Fig. 13 Mean stream-wise velocity at three locations in the near wake

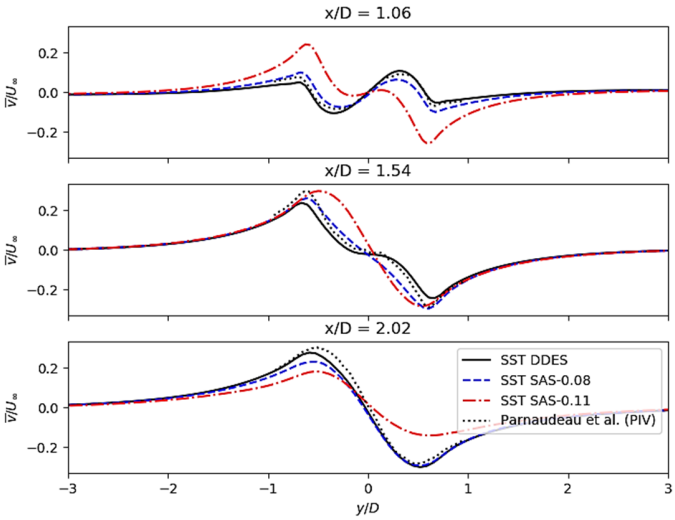

Fig. 14 Mean cross-flow velocity at three locations in the near wake

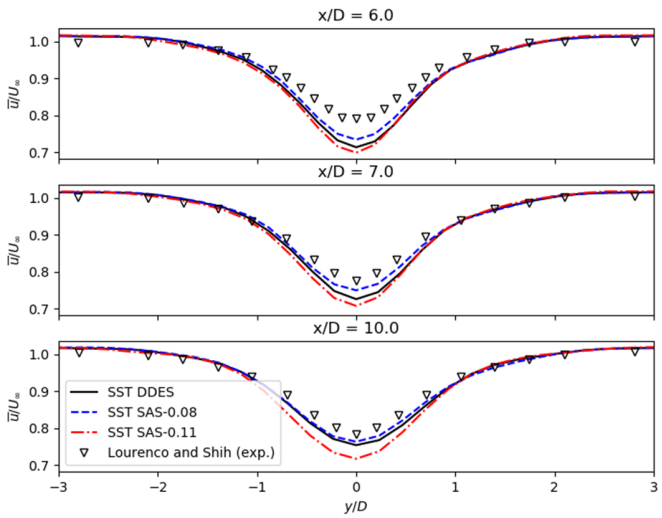

Fig. 15 Mean stream-wise velocity at three locations in the far wake

constant C_s = 0.11 contained in the L_{vk} limter is modified to be C_s = 0.08, SST-SAS is also able to achieve favorable performance in the coarse mesh. This observation stimulates the need to investigate how the L_{vk} limiter influences the performance of SST-SAS. What should be noticed is that the conclusions obtained in this paper is based on the case of Reynolds number 3900. Further investigations such as the cases of higher Reynolds number is needed in the future.

ACKNOWLEDGEMENTS

This work is supported by the National Natural Science Foundation of China (51490675, 11432009, 51579145), Chang Jiang Scholars Program (T2014099), Shanghai Excellent Academic Leaders Program (17XD1402300), Program for Professor of Special Appointment (Eastern Scholar) at Shanghai Institutions of Higher Learning (2013022), Innovative Special Project of Numerical Tank of Ministry of Industry and Information Technology of China (2016-23/09) and Lloyd's Register Foundation for doctoral student, to which the authors are most grateful.

REFERENCES

Egorov, Y, and Menter, F (2008). "Development and application of SST-SAS turbulence model in the DESIDER project," *Advances in Hybrid RANS-LES Modelling*, Berlin, Springer, 261-270.

Hunt, JCR, Wray, AA, and Moin, P (1988). "Eddies, streams, and convergence zones in turbulent flows," *Center for Turbulence Research Report CTR-S88*, Stanford University, USA, 193-208.

Kravchenko, AG, and Moin, P (2000). "Numerical studies of flow over a circular cylinder at Re_D = 3900," *Physics of Fluids*, 12(2), 403-417.

Menter, FR (2003). "Two-equation eddy-viscosity turbulence models for engineering applications," *AIAA Journal*, 2012, 32(8), 1598-1605.

Menter, FR, Kuntz, M, and Langtry, R (2003). "Ten years of industrial experience with the SST turbulence model," *Turbulence, Heat and Transfer*, 4(1), 625-632.

Menter, FR, and Egorov, Y (2005). "A Scale-Adaptive Simulation model using two equation models," *43rd AIAA Aerospace Sciences Meeting and Exhibit*, Reno, Ameraica, 1095-1107.

Menter, FR, and Egorov, Y (2010). "The Scale-Adaptive Simulation Method for Unsteady Turbulent Flow Predictions. Part 1: Theory and Model Description," *Flow Turbulence & Combustion*, 85(1),113-138.

Parnaudeau, P, Carlier, J, and Heitz, D, et al (2008). "Experimental and numerical studies of the flow over a circular cylinder at Reynolds number 3900," *Physics of Fluids*, 20(8), 287-12.

Rotta, JC (1968). "Über eine methode zur Berechnung turbulenter Scherströmungen," *aerodynamische Versuchsanstalt Göttingen*, Rep, 69 A14.

Smagorinsky, J (1963). "General circulation experiments with the primitive equations. I. The basic experiment," *Monthly Weather Review*, 91(3), 99-164.

Spalart, PR, Jou, WH, and Strelets, M, et al (1997). "Comments on the Feasibility of LES for Wings, and on a Hybrid RANS/LES Approach," *Advances in DNS/LES*, 1997, 1, 4-8.

Spalart, PR, Deck, S, and Shur, ML, et al (2006). "A New Version of Detached-eddy Simulation, Resistant to Ambiguous Grid Densities," *Theoretical & Computational Fluid Dynamics*, 20(3), 181-195.

Stamou, A, and Papadonikolaki, G (2014). "Modeling the 3-D flow around a cylinder using the SAS hybrid model," *Global Nest Journal*, 16(5), 901-918.

Zhao, WW, and Wan, DC (2016). "Numerical study of 3D flow past a circular cylinder at subcritical Reynolds number using SST-DES and SST-URANS," *Chinese Journal of Hydrodynamics*, 31(1), 1-8.

Zheng, W, Yan, C, and Liu, H, et al (2016). "Comparative assessment of SAS and DES turbulence modeling for massively separated flows," *Acta Mech*, 32(1), 12-21.